Mon. Not. R. Astron. Soc. **396,** 2405–2418 (2009) doi:10.1111/j.1365-2966.2009.14914.x

The evolution of the Lyα forest effective optical depth following He II reionization

James S. Bolton,[1]⋆ S. Peng Oh[2] and Steven R. Furlanetto[3]

[1]*Max Planck Institut für Astrophysik, Karl-Schwarzschild Str. 1, 85748 Garching, Germany*
[2]*Department of Physics, University of California, Santa Barbara, CA 93106, USA*
[3]*Department of Physics and Astronomy, University of California, Los Angeles, CA 90095, USA*

Accepted 2009 April 15. Received 2009 April 15; in original form 2009 January 23

ABSTRACT

Three independent observational studies have now detected a narrow ($\Delta z \simeq 0.5$) dip centred at $z = 3.2$ in the otherwise smooth redshift evolution of the Lyα forest effective optical depth. This feature has previously been interpreted as an indirect signature of rapid photoheating in the intergalactic medium (IGM) during the epoch of He II reionization. We examine this interpretation using a semi-analytic model of inhomogeneous He II reionization and high-resolution hydrodynamical simulations of the Lyα forest. We instead find that a rapid ($\Delta z \simeq 0.2$) boost to the IGM temperature ($\Delta T \simeq 10^4$ K) beginning at $z = 3.4$ produces a well understood and generic evolution in the Lyα effective optical depth, where a sudden reduction in the opacity is followed by a gradual, monotonic recovery driven largely by adiabatic cooling in the low-density IGM. This behaviour is inconsistent with the narrow feature in the observational data. If photoheating during He II reionization is instead extended over several redshift units, as recent theoretical studies suggest, then the Lyα opacity will evolve smoothly with redshift. We conclude that the sharp dip observed in the Lyα forest effective optical depth is instead most likely due to a narrow peak in the hydrogen photoionization rate around $z = 3.2$, and suggest that it may arise from the modulation of either reprocessed radiation during He II reionization, or the opacity of Lyman limit systems.

Key words: methods: numerical – intergalactic medium – quasars: absorption lines – cosmology: theory – diffuse radiation.

1 INTRODUCTION

Observations of the He II (Gunn & Peterson 1965) trough in the spectra of intermediate-redshift quasars, coupled with large fluctuations in the mean transmission of the He II Lyα forest, provide the most direct evidence for the tail end of He II reionization occurring around $z = 3$ (Jakobsen et al. 1994; Davidsen, Kriss & Wei 1996; Heap et al. 2000; Shull et al. 2004; Zheng et al. 2004; Fechner et al. 2006). However, to date only a handful of ultraviolet (UV) quasar spectra suitable for detailed analyses of the He II Lyα forest have been obtained (although see Syphers et al. 2009). Moreover, the Lyα transmission is sensitive to small He II fractions only, and is thus unsuitable for probing the earliest stages of He II reionization.

Fortunately, the impact of He II reionization on the intergalactic medium (IGM) can still be probed, albeit indirectly, over a wider redshift baseline with the existing wealth of high quality, high signal-to-noise ratio (S/N) H I Lyα forest data. First, the increased temperature of the IGM expected following He II reionization (Miralda-Escudé & Rees 1994; Abel & Haehnelt 1999; Paschos et al. 2007) will thermally broaden absorption lines in the Lyα forest (Haehnelt & Steinmetz 1998). There is some evidence that observed linewidths are consistent with a sudden increase in the IGM temperature around $z = 3.3$ (Ricotti, Gnedin & Shull 2000; Schaye et al. 2000), although the error bars on the measurements are large and not all studies agree on this result (McDonald et al. 2001). Secondly, the residual H I fraction in the IGM, which is in photoionization equilibrium with the metagalactic ultraviolet background (UVB), will be lowered through the temperature dependence of the H II recombination coefficient ($n_{\rm H\,I} \propto T^{-0.7}$). If the temperature of the IGM rises suddenly following He II reionization, a similarly sudden decrease in the H I fraction, and hence the observed Lyα forest opacity, will result (Theuns et al. 2002, hereafter T02; Bernardi et al. 2003; Faucher-Giguère et al. 2008a, hereafter FG08a).

Bernardi et al. (2003), in a study using 1061 moderate-resolution quasar spectra obtained from the Sloan Digital Sky Survey (SDSS), statistically measured such a departure from the otherwise smooth, power-law evolution of the Lyα forest opacity. A sudden decrease of around 10 per cent was observed in the effective optical depth at $z = 3.2$, followed by a recovery to its former power-law evolution by

⋆E-mail: jsb@mpa-garching.mpg.de

$z = 2.9$. FG08a have subsequently reconfirmed the Bernardi et al. (2003) result by using 86 high-resolution, high S/N spectra obtained with Keck/High Resolution Echelle Spectrometer (HIRES)/Echelle Spectrograph and Imager (ESI) and Magellan/MIKE (Magellan Inamori Kyocera Echelle) to directly measure the Lyα opacity. Furthermore, Dall'Aglio, Wisotzki & Worseck (2008) have also recently detected a narrow dip in the Lyα forest effective optical depth at $z = 3.2$, albeit at a low level of statistical significance (2.6σ), using another set of 40 high-resolution spectra obtained with Very Large Telescope/UV–Visual Echelle Spectrograph (VLT/UVES).

T02 compared detailed hydrodynamical simulations of the Lyα forest to the Bernardi et al. (2003) data and interpreted this feature as indirect evidence for photoheating during He II reionization. However, recent theoretical studies indicate it is difficult to explain this narrow feature in the Lyα opacity evolution by invoking a rapid temperature boost in the IGM alone. Bolton, Oh & Furlanetto (2009) used analytical and numerical arguments to demonstrate that there are too few hard photons available to heat the entire IGM by the required amount ($\sim 10^4$ K) over the time-scale on which the observed opacity decreases ($\Delta z = 0.1$–0.2). State-of-the-art radiative transfer simulations also indicate that He II reionization and reheating will be an extended rather than sudden process, with the volume averaged IGM temperature rising gradually from higher redshifts (McQuinn et al. 2009). A rapid injection of energy into the IGM during He II reionization is thus unlikely to explain the sharp initiation of the observed dip in the Lyα forest opacity.

Somewhat separate to this argument, however, is the explanation for the subsequent *recovery* of the observed Lyα opacity to its former power-law evolution by $z = 2.9$. Let us assume that the narrow dip in the Lyα forest effective optical depth is indeed initiated by a large, rapid temperature boost in the IGM following He II reionization (but see Bolton et al. 2009; McQuinn et al. 2009). Although this will not occur over the whole IGM, such rapid heating is not necessarily excluded in localized patches close to quasars with very hard spectra, where the requisite hard photons are abundant. Following reionization, the thermal evolution of the IGM at low density is dominated by the balance between photoheating and adiabatic cooling due to Hubble expansion (Hui & Gnedin 1997; Theuns et al. 1998). However, if the Lyα opacity evolution were driven by the thermal state of the IGM alone through the H II recombination rate, any subsequent recovery in the opacity due to adiabatic cooling would occur over a Hubble time – too long to explain the rapid recovery in the Bernardi et al. (2003) feature. The study of T02 instead demonstrated that this interpretation is too simplistic. They found that the hydrodynamical response of the IGM following a sudden reheating, coupled with the impact of the extra electrons liberated during He II reionization, are enough to drive the Lyα opacity back to its former power-law evolution by $z = 2.9$ as observed by Bernardi et al. (2003) – much earlier than one would expect using the simple argument above.

To date, the only dedicated study of the impact of He II reionization on the Lyα forest effective optical depth using high-resolution hydrodynamical simulations of the IGM has been performed by T02. McQuinn et al. (2009) recently presented a detailed analysis of the evolution of the Lyα forest opacity using radiative transfer simulations of He II reionization. However, their study necessarily used low-resolution, post-processed dark matter simulations, and they were thus unable to model the impact of the gas hydrodynamics on the recovery of the Lyα forest opacity. In light of these recent observational and theoretical results we therefore re-examine the impact of He II reionization on the evolution of the Lyα forest opacity using semi-analytic modelling and high-resolution hydrodynamical simulations of the IGM. In particular, we shall focus on the explanation for the *recovery* of the dip observed in the Lyα forest opacity. This paper is therefore closely related to the work presented in Bolton et al. (2009), where the issues surrounding the *initiation* of the feature first detected by Bernardi et al. (2003) (i.e. the plausibility, or lack of, for the rapid photoheating of the IGM) were examined in detail.

The structure of this paper is as follows. We begin in Section 2 with a brief review of the relationship between the Lyα forest opacity and the underlying physical properties of the IGM. In Section 3 we use a semi-analytic model to examine the evolution of the Lyα forest opacity following photoheating in the IGM during inhomogeneous He II reionization. Motivated by these results, we then proceed to model the Lyα forest opacity in more detail using hydrodynamical simulations of the IGM. The simulations are described in Section 4, and the evolution of the Lyα forest opacity in the simulations is presented in Section 5. In Section 6 we investigate the impact of sudden reheating on the IGM gas distribution and peculiar velocity field; we find that our simulations are unable to reproduce the narrow feature observed in the Lyα forest opacity evolution. Finally, we consider alternative explanations for the observational data in Section 7 before concluding in Section 8.

2 THE FLUCTUATING GUNN–PETERSON APPROXIMATION (FGPA)

The forest of Lyα absorption lines observed in the spectra of high-redshift quasars originates from the neutral hydrogen remaining in the intervening, low-density IGM following H I reionization (Bi, Boerner & Chu 1992; Zhang, Anninos & Norman 1995; Hernquist et al. 1996; Miralda-Escudé et al. 1996; Theuns et al. 1998). The mean normalized flux of the Lyα forest, $\langle F \rangle = \langle I_{\rm observed}/I_{\rm emitted} \rangle$, is the simplest observable quantity, and it is often expressed as an effective optical depth,

$$\tau_{\rm eff} = -\ln\langle F \rangle \equiv -\ln\langle {\rm e}^{-\tau} \rangle, \quad (1)$$

where τ is the underlying Lyα optical depth in each pixel of the spectrum or spectra from which $\langle F \rangle$ is measured. Assuming the IGM is highly ionized and in photoionization equilibrium with the metagalactic UVB, and the low-density IGM ($\Delta = \rho/\langle\rho\rangle \leq 10$) follows a power-law temperature–density relation, $T = T_0 \Delta^{\gamma-1}$ (Hui & Gnedin 1997; Valageas, Schaeffer & Silk 2002), the Lyα optical depth at $z \gtrsim 2$ may be written as (e.g. Weinberg et al. 1999; McDonald & Miralda-Escudé 2001)

$$\tau \simeq 1.0 \frac{(1+\chi_{\rm He})}{\Gamma_{-12}} \left(\frac{T_0}{10^4\,{\rm K}}\right)^{-0.7} \left(\frac{\Omega_{\rm b}\,h^2}{0.024}\right)^2 \left(\frac{\Omega_{\rm m}\,h^2}{0.135}\right)^{-1/2} \times \left(\frac{1+z}{4}\right)^{9/2} \Delta^{2-0.7(\gamma-1)}, \quad (2)$$

where $\Omega_{\rm b}$ and $\Omega_{\rm m}$ are the present day baryon and matter densities as a fraction of the critical density, $h = H_0/100\,{\rm km\,s^{-1}\,Mpc^{-1}}$ for the present day Hubble constant H_0, $\Delta = \rho/\langle\rho\rangle$ is the normalized gas density, T_0 is the gas temperature at mean density, γ is the slope of the temperature–density relation and $\Gamma_{-12} = \Gamma_{\rm H\,I}/10^{-12}\,{\rm s^{-1}}$ is the hydrogen photoionization rate. The power-law temperature dependence is due to the case-A H II recombination coefficient, and $\chi_{\rm He}$ accounts for the extra electrons liberated during He II reionization; $\chi_{\rm He} = 1.08$ prior to He II reionization and $\chi_{\rm He} = 1.16$ afterwards for a helium fraction by mass of $Y = 0.24$ (Olive & Skillman 2004). The effective optical depth can then be estimated by integrating over all possible IGM densities Δ.

Equation (2) is the FGPA, and although it ignores the effect of redshift space distortions on the Lyα forest opacity, it clearly elucidates the relationship between the opacity and the underlying physical properties of the IGM. A sudden decrease in the Lyα effective optical depth (e.g. Bernardi et al. 2003) can thus be attributed to an increase in the IGM temperature, either by raising T_0 or changing γ,[1] an increase in the photoionization rate, or a combination of both. On the other hand, an increase in the free electron fraction will raise the opacity by reducing the recombination time-scale. Both an increase in the IGM temperature and an 8 per cent change in the free electron fraction will be associated with He II reionization. Keeping these points in mind, we now proceed to describe a semi-analytical model for inhomogeneous He II reionization which utilizes this useful approximation.

3 THE Lyα FOREST OPACITY DURING INHOMOGENEOUS He II REIONIZATION

3.1 A semi-analytic model

Before analysing our detailed hydrodynamical simulations, we first consider a simplified semi-analytic model which illustrates the difficulty of reproducing the localized feature observed by Bernardi et al. (2003) in the Lyα forest. Although this model is unable to compute many of the detailed properties of the Lyα forest (such as line broadening and the impact of peculiar velocities), it has the virtue of including inhomogeneous reionization (Furlanetto & Oh 2008a), which our hydrodynamical simulations do not. The model is based on the calculations presented in Furlanetto & Oh (2008b), who examined how He II reionization can affect the temperature–density relation of the IGM, and we refer the reader there for more details.

In brief, the model has three parts. The first determines the reionization history of gas elements of a given density in the IGM (Furlanetto & Oh 2008b). For most of our calculations, we assume that the probability that an element is reionized at any particular time is independent of its density, simply tracing the mean ionization history, $\bar{x}_{\rm i}(z)$. We also compare to a 'density-driven' model in which high-density regions are ionized first (because they sit near the biased regions that host quasars). However, recent numerical simulations of He II reionization suggest that the ionized regions are large and rare enough that this correlation is weak (McQuinn et al. 2009), so we usually use the density-independent model. We will assume that He II reionization ends at $z_{\rm He} = 3.2$, consistent with the calculations below, and that hydrogen reionization (which only affects the temperature of gas for which helium is still singly ionized) occurs at $z_{\rm H} = 8$; the latter has little effect on our calculation.

To make this comparison as straightforward as possible, we assume that $\bar{x}_{\rm i}(z)$ is simply proportional to the mass in galaxies with $m \gtrsim 5 \times 10^{11}\,{\rm M}_{\odot}$ (in other words, these massive galaxies contain supermassive black holes that have gone through bright quasar phases). This provides a reasonable approximation to the quasar emissivity (compared to e.g. the luminosity function of Hopkins, Richards & Hernquist 2007) and also leads to fast He II reionization, with over 70 per cent of the ionization occurring after $z = 4.2$, if He II reionization ends at $z = 3.2$ (Furlanetto & Oh 2008a).

The second ingredient is to follow the thermal evolution of each gas element after reionization. We again use the method presented in Furlanetto & Oh (2008b), which is in turn based on Hui & Gnedin (1997). We include all of the relevant atomic cooling, heating, recombination and photoionization processes, as well as adiabatic expansion (and collapse for overdense regions). After reionization, the dominant processes are photoheating and adiabatic cooling, which together determine the asymptotic, nearly power law, temperature–density relation (Hui & Gnedin 1997; Hui & Haiman 2003).

The chief uncertainty in this model is the initial temperature after reionization, $T_{\rm i}$, which depends in a non-trivial manner on the spectrum of the photons ionizing the gas parcel (Abel & Haehnelt 1999; Paschos et al. 2007; Tittley & Meiksin 2007; Bolton et al. 2009; McQuinn et al. 2009). This may itself be inhomogeneous in the IGM, because low-energy photons will be absorbed near their hosts, leaving many of the ionizations to be done by hard photons (Abel & Haehnelt 1999). We therefore consider a range of possibilities for $T_{\rm i}$. Our fiducial model takes $T_{\rm i} = 4 \times 10^4\,{\rm K}$, larger than is typically expected in order to exaggerate the effect of heating (e.g. Bolton et al. 2009; McQuinn et al. 2009).

Finally, in order to compute the average optical depth we need to assume an IGM density distribution, $P_V(\Delta)$ (averaged by volume), as well as the distribution of temperatures and ionization rates at each density. We will use the density distribution recommended by Miralda-Escudé, Haehnelt & Rees (2000):

$$P_V(\Delta)\,{\rm d}\Delta = A_0 \Delta^{-\beta} \exp\left[-\frac{(\Delta^{-2/3} - C_0)^2}{2(2\delta_0/3)^2}\right] {\rm d}\Delta. \quad (3)$$

This form fits cosmological simulations at $z = 2$–4 quite well. Note that the underlying simulation had somewhat different cosmological parameters than the currently preferred values; it is, however, accurate enough for the qualitative calculations that follow.

3.2 The Lyα effective optical depth

To compute the Lyα effective optical depth, we assign each volume element of known density an optical depth according to equation (2).[2] Our model makes no predictions about the amplitude of the ionizing background, and for simplicity we set $\Gamma_{-12} = 1$ over the entire redshift range $z = 2$–5. This is consistent with constraints derived by comparing observational data to simulations of the Lyα forest at $2 \leq z \leq 4$ (Bolton et al. 2005), and yields a mean transmission reasonably close to the observed values.

We choose the temperatures by following gas elements of the appropriate density after their most recent reionization event using the thermal evolution code described above, with the reionization redshifts distributed according to the overall ionization history. We

[1] Lowering (raising) the value of γ will increase the temperature in underdense (overdense) regions of the IGM while decreasing the temperature in overdense (underdense) regions. Whether raising or lowering γ subsequently decreases the effective optical depth of the Lyα forest thus depends on redshift. At $z \geq 3$ the Lyα forest opacity is mainly sensitive to underdense regions in the IGM. Lowering γ therefore decreases the Lyα effective optical depth at $z \geq 3$ by producing hotter, more highly ionized voids (e.g. Bolton et al. 2005; Faucher-Giguère et al. 2008b). Typical values adopted for γ in Lyα forest models lie in the range $1 \leq \gamma \leq 1.6$, although there is some evidence to suggest a more complex relationship between temperature and density, perhaps with $\gamma < 1$, may be required to reproduce the observed Lyα forest flux distribution (Becker, Rauch & Sargent 2007; Bolton et al. 2008).

[2] We drop the assumption of a power-law temperature–density relation in this instance; see Furlanetto & Oh (2008b) for some example temperature distributions.

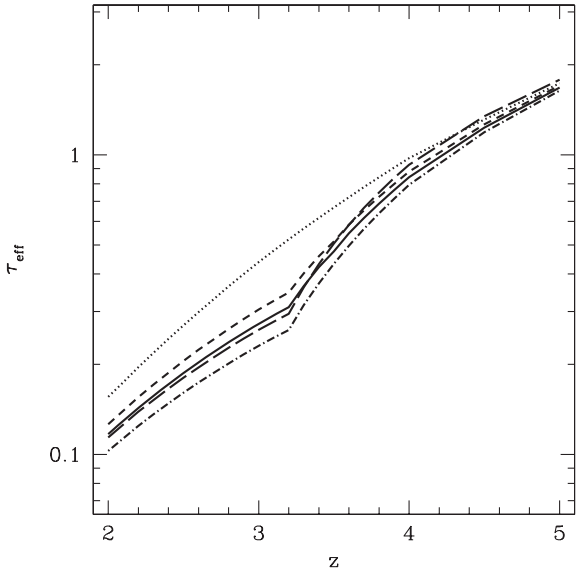

Figure 1. Mean transmission histories in our semi-analytic models. The dotted curve shows $\tau_{\rm eff}(z)$ if we ignore He II reionization and set $T = 20\,000$ K throughout. The other curves include He II reionization at $z_{\rm He} = 3.2$, as described in the text. The short-dashed, solid and dot–dashed curves assume $T_{\rm i} = (3, 4, 6) \times 10^4$ K, respectively. The long-dashed curve assumes $T_{\rm i} = 4 \times 10^4$ K but that reionization proceeds from high to low densities.

then calculate

$$e^{-\tau_{\rm eff}} = \int_0^\infty {\rm d}\Delta\, P_V(\Delta) \int {\rm d}T\, P(T|\Delta)\, e^{-\tau(T,\Delta)}, \quad (4)$$

where $P(T|\Delta)$ is the probability distribution of temperatures for elements at density Δ and $\tau_{\rm eff}$ is the effective optical depth. Again, we emphasize that this ignores peculiar velocities of the gas, line blending (and indeed the wings of every line) and the clustering of the absorbers, but it provides a qualitative description of the evolving transmission.

Fig. 1 shows some example histories computed in this manner. As a basis for comparison, the dotted curve ignores He II reionization and assumes a constant ionizing background and IGM temperature ($T = 20\,000$ K). This does not quantitatively match the observed evolution; it merely serves to show that, without He II reionization, our model produces smooth, nearly featureless evolution.

The other curves assume that helium reionization ends at $z_{\rm He} = 3.2$. The short-dashed, solid and dot–dashed curves assume $T_{\rm i} = (3, 4, 6) \times 10^4$ K, respectively (all relatively large in order to exaggerate the effect; see Bolton et al. 2009; McQuinn et al. 2009 for self-consistent estimates of the plausible temperature range). The long-dashed curve takes $T_{\rm i} = 4 \times 10^4$ K and assumes that reionization is density dependent (Furlanetto & Oh 2008b); this aspect of reionization has only a small effect on the mean transmission. This is because the Lyα forest is sensitive to only a narrow range of densities near the mean, where the density modulation is modest anyway.

According to these models, He II reionization can certainly induce a feature in $\tau_{\rm eff}$, so long as the temperature increase is large enough. In all cases, $\tau_{\rm eff}$ falls relatively steeply until $z_{\rm He}$ before levelling off and returning closer to the expected evolution without He II reionization. The shape is generic within these reionization models, although note that the downward turn in $\tau_{\rm eff}$ is still significantly shallower than that observed in the observational data (Bernardi et al. 2003; FG08a). The pre-reionization phase can be steepened by making reionization occur faster, but the model assumed here is not far from empirical estimates of the evolution of the quasar emissivity. Moreover, compressing He II reionization into a short time interval limits the temperature jump that it can induce, because the photoionization time-scale associated with high-energy photons (which provide the most efficient heating) is quite long (Bolton et al. 2009).

However, the post-reionization evolution is completely generic and easy to understand. In this regime, the thermal evolution is dominated by the competition between photoheating and cooling by adiabatic expansion. The time-scale for the cooling is therefore the expansion, or Hubble, time – a substantial fraction of the age of the Universe. There is no way to avoid this behaviour for the temperature history, and to the extent that the Lyα forest depends only on these temperatures, He II reionization cannot induce a *narrow* feature in the transmission which recovers quickly to its pre-reionization evolution.

Of course, we have emphasized that the forest is indeed more complex than this model, because of peculiar velocities, geometric effects and line blending. In principle, these can induce a narrower feature, and T02 appealed to just such an effect to explain the Bernardi et al. (2003) feature. In their simulations, once the reheated gas in the IGM became overpressurized with respect to its surroundings it started to expand, resulting in a sudden change in the peculiar velocity gradients in the IGM. This extended the Lyα absorption lines in redshift space by shifting absorption from the saturated line cores to the wings, increasing the line equivalent widths and hence the mean Lyα opacity. In the remainder of this paper, we will examine all of these effects in more detail using new hydrodynamical simulations that do include a detailed reconstruction of the Lyα forest.

4 HYDRODYNAMICAL SIMULATIONS OF THE Lyα FOREST

4.1 Initial conditions

The hydrodynamical simulations in this study are performed using an upgraded version of the publicly available parallel Tree-SPH (smoothed particle hydrodynamics) code GADGET-2 (Springel 2005). All simulations have a box size $15\,h^{-1}$ comoving Mpc and contain 2×400^3 gas and dark matter particles. The mass of each gas particle is $9.4 \times 10^5\,{\rm M}_\odot$ and the gravitational softening length is 1/30th of the mean linear interparticle spacing. This adequately resolves the Lyα forest at $2 \le z \le 4$ (Theuns et al. 1998; Bolton et al. 2008) and provides just over twice the mass resolution of the simulations used in the T02 study.[3] Star formation is included using a simplified prescription which converts all gas particles with overdensity $\Delta > 10^3$ and temperature $T < 10^5$ K into collisionless stars, significantly speeding up the simulations. Outputs are saved every $\Delta z = 0.05$ in the redshift range $2 \le z \le 4$, enabling a very fine sampling of the simulation data with redshift.

The ionization state of the gas particles is computed in the optically thin limit using a non-equilibrium ionization algorithm which follows the abundances of six species: H I, H II, He I, He II, He III and e^- (Bolton & Haehnelt 2007a). The UVB model of Haardt & Madau (2001, hereafter HM01) including emission from quasars

[3] T02 use a modified version of HYDRA (Couchman, Thomas & Pearce 1995) to run hydrodynamical simulations in a $12\,h^{-1}$ comoving Mpc box with a gas particle mass of $2.0 \times 10^6\,{\rm M}_\odot$.

and galaxies is used to compute the H I, He I and He II photoionization and heating rates. This model is in good agreement with observational constraints on the metagalactic H I photoionization rate (Tytler et al. 2004; Bolton et al. 2005), although we set the HM01 photoionization and heating rates for all species to zero at $z > 6$ in order to match the simulations of T02.

The UVB is assumed to be spatially uniform in all our simulations. This will be a reasonable approximation at the H I photoionization edge at $z < 4$, when the mean free path for hydrogen ionizing photons is much larger than the average separation between ionizing sources (Bolton & Haehnelt 2007b; Faucher-Giguère et al. 2008b; Furlanetto 2008). However, a full radiative transfer implementation is required to model the impact of inhomogeneous He II reionization on the Lyα forest opacity (e.g. Maselli & Ferrara 2005; Paschos et al. 2007; Tittley & Meiksin 2007; Bolton et al. 2009; McQuinn et al. 2009). Although He II reionization does not *directly* impact Lyα forest effective optical depth, our simulations do not capture the effect of the resulting fluctuations in the IGM temperature, which do impact on the effective optical depth through the temperature dependence of the H II recombination coefficient. However, our simulation volume is $15\,h^{-1}$ comoving Mpc, which is small on comparison to the ∼50 comoving Mpc scales on which large temperature fluctuations are expected (McQuinn et al. 2009). Although not ideal, our assumption of instantaneous reheating on this smaller scale is therefore a reasonable approximation. Furthermore, note that HM01 implicitly assumes that He II is reionized at all redshifts, i.e. He II only exists in the dense Lyα absorbers which they model. Radiative transfer effects obviously modify the form of the UVB prior to He II reionization (e.g. Madau & Haardt 2009), both in He II ionizing radiation above 4 Ry and in reprocessed radiation from He II Lyman series and two photon emission. Thus, the UVB could be quite different before reionization is complete. We comment on this more in Section 7.2.

The simulations were all started at $z = 99$, with initial conditions generated using the transfer function of Eisenstein & Hu (1999). The cosmological parameters adopted are $\Omega_{\rm m} = 0.26, \Omega_\Lambda = 0.74$, $\Omega_{\rm b}\,h^2 = 0.024, h = 0.72, \sigma_8 = 0.85$ and $n_{\rm s} = 0.95$. These are consistent with the fifth year *Wilkinson Microwave Anisotropy Probe* (*WMAP*) data (Dunkley et al. 2009), aside from a slightly larger value for the matter power spectrum normalization. The gas is assumed to be of primordial composition with a helium mass fraction of $Y = 0.24$ (e.g. Olive & Skillman 2004).

4.2 Thermal and ionization histories

Five hydrodynamical simulations, listed in Table 1, were performed for this study. The simulations use different models for the thermal and ionization evolution of the IGM, but aside from the S3 model, which we shall discuss later, are identical in all other respects. The different thermal histories are constructed by increasing the HM01 He II photoheating rate in the simulations (e.g. T02; Bolton et al. 2005; Jena et al. 2005). This mimics spectral hardening due to radiative transfer effects during He II reionization by boosting the mean excess energy per He II photoionization (Abel & Haehnelt 1999; Bolton, Meiksin & White 2004). Note that we only model the jump in heating rates, which affects the thermal evolution; apart from model S2 which we discuss below, we do not model the jump in the He II fraction itself.

Table 1. Hydrodynamical simulations used in this study. All the simulations have a box size of $15\,h^{-1}$ comoving Mpc and contain 2×400^3 gas and dark matter particles.

Model	Thermal history description
S1	Sharp temperature boost
E1	Extended temperature boost
N1	No temperature boost; control model
S2	Similar to S1, but with a rapid change in $n_{\rm e}$
S3	Identical to S1, but with a stricter time-step limit

The IGM temperatures at mean density, T_0, in all five simulations are displayed in the left-hand panel of Fig. 2 as a function of redshift. These data are compared to observational constraints obtained by Schaye et al. (2000) from an analysis of absorption linewidths in the Lyα forest. Note that these thermal histories are not fits to the observational data; they are instead merely chosen to be representative of IGM thermal histories presented in the literature. The S1 model (solid curve) closely resembles the T_0 evolution in the simulations of T02, with a sudden increase ($\Delta z = 0.1$) in temperature, $\Delta T \sim 10^4$ K, beginning at $z = 3.4$. Note that this temperature boost occurs over a much shorter time-scale than that in our semi-analytical model of He II reionization (Furlanetto & Oh 2008b). The E1 model (dot–dashed curve) is qualitatively similar to recent results from detailed three-dimensional radiative transfer simulations of He II reionization (McQuinn et al. 2009). The temperature boost develops over a longer time-scale as quasars gradually photoheat the IGM. The third simulation, N1 (dotted curve), is included as a control model, and has no temperature boost.

The corresponding volume weighted He II and H I fractions in the simulations are displayed in the central panel of Fig. 2. In the S1, E1 and N1 simulations, both H I and He II reionization commence at $z = 6$. This choice is deliberate; these three models are designed to exclude the 8 per cent increase in the free electron fraction following He II reionization (see discussion in Section 2). Instead, they will be used to explore the impact of differences in the IGM thermal state *alone* on the $\tau_{\rm eff}$ evolution. Sudden He II reionization at $z = 3.4$ is instead included in a fourth model, S2 (long-dashed curve), which is tailored to have a similar temperature at mean density to the S1 model. The S2 simulation is therefore the most similar to the model used by T02, who also assumed H I reionization at $z = 6$ and He II reionization at $z = 3.4$.

The right-hand panel in Fig. 2 displays the evolution of the slope of the temperature–density relation, $T = T_0\Delta^{\gamma-1}$ (Hui & Gnedin 1997; Valageas et al. 2002), in each of the simulations. The power-law index γ gradually increases towards lower redshifts in the E1 and S1 models, asymptotically approaching the upper limit of $\gamma \sim 1.6$ achieved by the balance between photoheating and adiabatic cooling in the low-density IGM. Note, however, the S1 and S2 models, although having very similar T_0 values, exhibit different behaviour for γ. This is due to the different ionization histories adopted in the two models. During the reionization of He II at $z = 3.4$ in the S2 model, photoionization equilibrium is no longer a good assumption and the He II photoheating rate is *independent* of density (Bolton et al. 2009). This is because the He II fraction – $f_{\rm He\,II} = n_{\rm He\,II}/n_{\rm He} \sim 1$ immediately prior to reionization – is independent of density. This flattens the temperature–density relation and lowers the value of γ. However, in the S1 model, where the He II is already in ionization equilibrium with the UVB, the He II photoheating rate is instead *proportional* to the IGM density (Theuns 2005). The He II fraction is proportional to density (due to higher recombination rates in denser regions) and the extra energy injected at $z = 3.4$ instead increases γ. As we shall see, these differences will also play a small role (relative to T_0) in the simulated $\tau_{\rm eff}$ evolution. These values are compared to measurements of γ from Schaye et al.

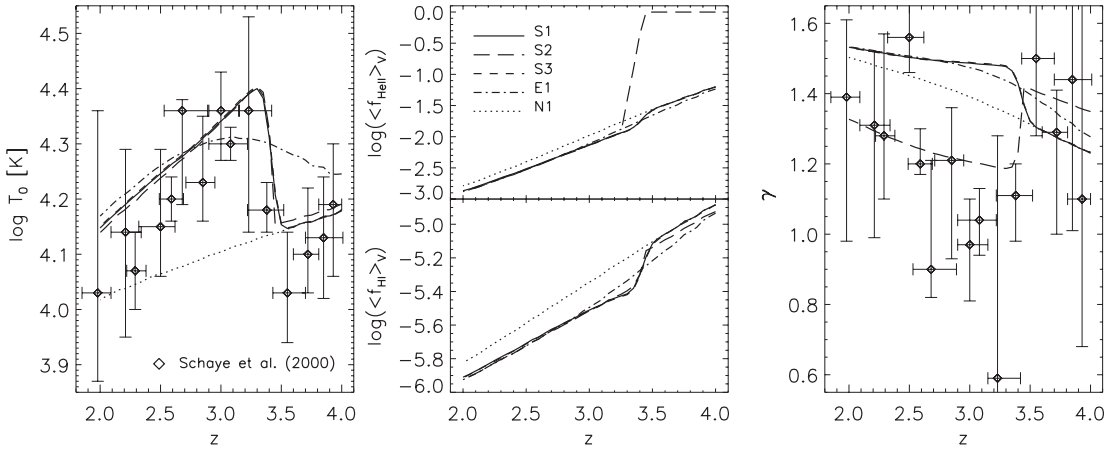

Figure 2. Left: the temperature of the IGM at mean density, T_0, in the five simulations used in this study: S1 (solid curve), S2 (long-dashed curve), S3 (short-dashed curve), E1 (dot–dashed curve) and N1 (dotted curve). The temperatures are given at intervals of $\Delta z = 0.05$ over the redshift range $2 \leq z \leq 4$. These data are compared to observational constraints obtained by Schaye et al. (2000) from an analysis of absorption linewidths in the Lyα forest. Centre: the corresponding volume weighted He II (upper panel) and H I (lower panel) fractions. Right: the slope of the power-law temperature–density relation, $T = T_0\Delta^{\gamma-1}$. The values are obtained by a least-squares power-law fit to the volume weighted temperature–density plane in the simulations at $0.1 \leq \Delta \leq 1$ and $T \leq 10^5$ K. The data are again compared to observational constraints from Schaye et al. (2000). Note that the S1 and S3 models are almost indistinguishable in all three panels.

(2000). Although the error bars are large, somewhat lower values of γ are preferred at $z < 3.5$.

4.3 Time integration in GADGET-2 and HYDRA

We run the fifth and final model, S3, to quantify the effect of the GADGET-2 time integration scheme on our results. The study of T02 used hydrodynamical simulations performed with a modified version of the P^{3}M-SPH code HYDRA (Couchman et al. 1995). HYDRA employs a single step time integration scheme where all particle positions are advanced on the minimum time-step required throughout the simulation volume. In contrast, GADGET-2 uses individual time-steps for each particle. This means that particles in high-density regions, where dynamical time-scales are short, have time-steps which are orders of magnitude smaller than particle time-steps in the lowest density regions (Springel 2005). This enables efficient use of computational resources and substantially improves code performance. However, if a sudden boost to the IGM temperature occurs in the middle of a particle time-step, the energy injected will be smeared over the time-scale corresponding the particle time-step. In regions where the dynamical time-scale is long, such as the low-density IGM which dominates the transmission in the Lyα forest at $z = 3$, this can delay the impact photoheating on the gas and could potentially affect our numerical results.

Unfortunately, forcing a single minimum time-step in GADGET-2 to test this possibility would be prohibitively expensive. We instead impose a stricter upper limit on the maximum time-step size for *all* particles in the S3 model. In our first four simulations, the maximum allowed time-step for all particles is $\Delta \ln [1/(1+z)] = 0.05$, although in practice this value will vary and can be up to a factor of 2 smaller at any given redshift. This is equivalent to specifying the maximum allowed time-step as a fraction of the current Hubble time in the simulations. In the S3 model we instead impose a maximum time-step of $\Delta \ln [1/(1+z)] = 0.001$ at $z < 4.2$. This choice should provide a useful test of the impact of time-stepping on the gas hydrodynamics during a rapid change in the IGM temperature (V. Springel, private communication). The thermal and ionization history of the S3 model corresponds to the short-dashed curves in Fig. 2. Note the differences between the thermal and ionization histories of the S1 and S3 models are minimal, and that the curves are almost indistinguishable in all three panels.

5 THE LYα EFFECTIVE OPTICAL DEPTH FROM HYDRODYNAMICAL SIMULATIONS

5.1 Construction of synthetic Lyα spectra

We now turn to analysing the Lyα forest effective optical depth in each of our simulations. Synthetic Lyα forest spectra are constructed from each simulation by extracting randomly selected sightlines parallel to the simulation box boundaries at redshift intervals of $\Delta z = 0.05$ over the range $2 \leq z \leq 4$. At each redshift a total of 1024 sightlines are extracted, each with 1024 pixels. Every pixel in each sightline has a neutral hydrogen number density $n_{\rm H\,I}$, temperature T, peculiar velocity $v_{\rm pec}$ and Hubble velocity $v_{\rm H}$ associated with it. A standard SPH interpolation procedure (e.g. Theuns et al. 1998) is used to extract the first three of these quantities from the simulation data. In each line of sight with N pixels, the Lyα optical depth in pixel i is then given by

$$\tau(i) = \frac{c\sigma_\alpha \delta R}{\pi^{1/2}} \sum_{j=1}^{N} \frac{n_{\rm H\,I}(j)}{b_{\rm H\,I}(j)} H(a,x). \quad (5)$$

Here $b_{\rm H\,I} = (2k_{\rm B}T/m_{\rm H})^{1/2}$ is the Doppler parameter, $\sigma_\alpha = 4.48 \times 10^{-18}$ cm^2 is the Lyα cross-section, δR is the pixel width and $H(a, x)$ is the Voigt–Hjerting function (Hjerting 1938):

$$H(a,x) = \frac{a}{\pi} \int_{-\infty}^{\infty} \frac{{\rm e}^{-y^2}}{a^2 + (x-y)^2}\, {\rm d}y, \quad (6)$$

where $x = [v_{\rm H}(i) - u(j)]/b_{\rm H\,I}(j), u(j) = v_{\rm H}(j) + v_{\rm pec}(j), a = \Lambda_\alpha \lambda_\alpha / 4\pi b_{\rm H\,I}(j)$, $\Lambda_\alpha = 6.265 \times 10^8$ s^{-1} is the damping constant and $\lambda_\alpha = 1215.67$ Å is the wavelength of the Lyα transition. We use the analytic approximation for $H(a, x)$ provided by Tepper García (2006).

5.2 Comparison to the $\tau_{\rm eff}$ evolution observed by FG08a

We shall compare our simulation data to the recent direct measurement presented by FG08a, who found a feature in the Lyα forest opacity evolution consistent with the one detected statistically by Bernardi et al. (2003). FG08a measured $\tau_{\rm eff}$ over the redshift range $2 \leq z \leq 4.2$ using a sample of 86 high-resolution, high S/N quasar spectra obtained using three different instruments; the ESI and HIRES spectrographs on Keck and the MIKE spectrograph on Magellan.

We first renormalized the optical depths of the synthetic spectra by the same constant at every redshift, $A = 0.87$, to approximately match the normalization of the Lyα effective optical depth measured by FG08a. For a set of spectra with N pixels

$$\mathrm{e}^{-\tau_{\rm eff}} = \langle F \rangle = \frac{1}{N} \sum_{i=1}^{N} \mathrm{e}^{-A\tau_i}, \tag{7}$$

where τ_i is the optical depth in each pixel of the synthetic spectra and $\langle F \rangle$ is the mean observed flux. From equation (2), this renormalization corresponds to a straightforward rescaling of Γ_{-12} upwards by around 15 per cent if all other parameters in the simulation remain fixed. We have verified this renormalization has no impact on the shape of the $\tau_{\rm eff}$ evolution.

Fig. 3 shows the comparison between the $\tau_{\rm eff}$ evolution measured from our synthetic spectra and the observational data of FG08a. Note we have yet not processed the synthetic spectra to resemble the FG08a data (aside from the overall renormalization); the synthetic spectra are noiseless and have a substantially longer path-length than the observational data, but nevertheless provide a useful illustration of the $\tau_{\rm eff}$ evolution in the simulations. The solid, dotted and dashed curves display the S1, S2 and S3 models, respectively.

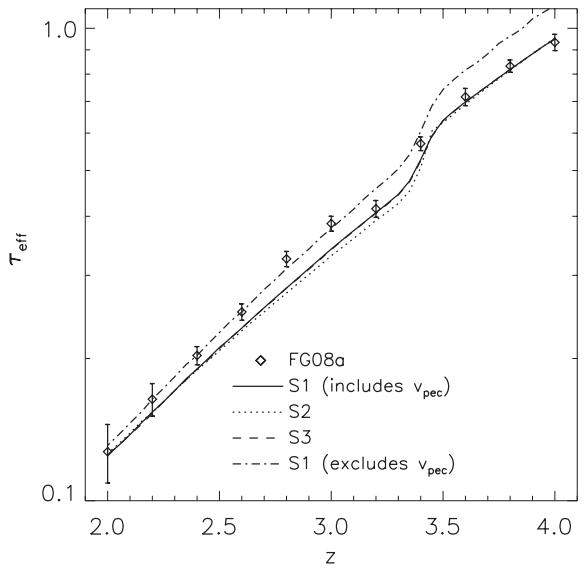

Figure 3. Comparison of $\tau_{\rm eff}$ measured from our synthetic Lyα forest spectra to the observational data of FG08a (open diamonds). The error bars correspond to the statistical uncertainties only. The synthetic data correspond to the models with a sharp temperature boost at $z = 3.4$ (S1, solid curve), an 8 per cent increase in the free electron fraction in addition to the sharp temperature boost (S2, dotted curve) and a stricter upper limit on the particle time-steps (S3, dashed curve). The latter model is indistinguishable from the S1 data. A fourth curve (dot–dashed) corresponds to the effective optical depth measured from the S1 model ignoring the effect of peculiar velocities on the Lyα forest. As noted by T02, neglecting peculiar velocities raises the absolute value of $\tau_{\rm eff}$ by deblending absorption lines.

These data all display the same generic features observed in the semi-analytic model; a downturn in $\tau_{\rm eff}$ due to the reheating of the IGM, followed by a slow recovery driven mainly by adiabatic cooling. In all instances it is clear the simulated data do not exhibit the narrow feature observed in the FG08a data.

First, note the S3 and S1 models are again almost indistinguishable, giving us confidence that the adaptive time integration scheme used in GADGET-2 will not significantly alter our results. Secondly, a small difference between the $\tau_{\rm eff}$ evolution observed in the S1 and S2 models is apparent at $z < 3.4$ – recall that the S2 simulation includes the 8 per cent increase in the free electron abundance due to sudden He II reionization. As noted in Section 2, the extra electrons will reduce the H II recombination time-scale and thus increase the Lyα opacity. In a highly ionized IGM the equilibration time-scale is $t_{\rm eq} \simeq f_{\rm H\,I} t_{\rm rec}$, where $f_{\rm H\,I} = n_{\rm H\,I}/n_{\rm H}$ is the IGM H I fraction and the recombination time-scale is

$$t_{\rm rec} \simeq \frac{9.4 \times 10^9\,{\rm yr}}{(1+\chi_{\rm He})\Delta} \left(\frac{T}{2 \times 10^4\,{\rm K}}\right)^{0.7} \left(\frac{1+z}{4}\right)^{-3}. \tag{8}$$

Therefore, for $f_{\rm H\,I} \simeq 10^{-5.5}$, the equilibration time-scale is already very short at mean density, $t_{\rm eq} \sim 3 \times 10^4$ yr (cf. 2.9×10^8 yr between $z = 3.4$ and 3), and the increase in $f_{\rm H\,I}$ (and hence $\tau_{\rm eff}$) following the additional 8 per cent increase in the electron number density should be very rapid. However, we instead find $\tau_{\rm eff}$ in the S2 model is 3–4 per cent *lower* than the S1 model at $3 \leq z \leq 3.4$. In this instance the effect of the extra electrons on the Lyα opacity is countered by the associated flattening of the temperature–density relation following sudden, homogeneous He II reionization. Recall that most of the Lyα forest at $z > 3$ is dominated by transmission from underdense regions in the IGM, which become hotter in the S2 model as the temperature–density relation flattens. Consequently, including a sudden change in the ionization state of He II in addition to a large temperature boost *increases* rather than decreases the magnitude of the dip in $\tau_{\rm eff}$ at $z < 3.4$. The extra electrons therefore do not help in reproducing the $\tau_{\rm eff}$ data in our model.

The fourth, dot–dashed curve corresponds to spectra extracted from the S1 simulation, but this time excluding the effect of redshift space distortions induced by peculiar velocities in the IGM. As noted by T02, excluding the peculiar velocities tends to deblend Lyα absorption lines, increasing $\tau_{\rm eff}$. It is also apparent the peculiar velocity field flattens the $\tau_{\rm eff}$ evolution somewhat; the gradient of the dot–dashed curve is steeper in comparison to the S1 data including peculiar velocities, especially at $z < 3$. These differences decrease towards lower redshift, indicating line blending becomes less widespread as the line number density and Lyα opacity both fall. However, in contrast to T02 (see their fig. 2), we find these redshift space distortions are insufficient to produce the rapid upturn in $\tau_{\rm eff}$ by $z = 2.9$ seen in the observational data. The redshift space distortions induced by peculiar velocities provide no change in the generic shape of the $\tau_{\rm eff}$ evolution with redshift. We have verified that this also holds for the S3 model with the stricter time-step limit. This result will be considered in more detail in Section 6.

However, to make a fair comparison to the FG08a data, our synthetic spectra must be processed to resemble their observational data set as closely as possible. Our renormalized synthetic spectra are therefore also convolved with a Gaussian instrument profile and resampled on to pixels of the required size. Gaussian distributed random noise is then added to each pixel. The parameters used for this procedure are summarized in Table 2, corresponding to the three instruments used in the FG08a data set. A random subsample of synthetic HIRES, ESI and MIKE spectra with a total path-length corresponding to the values displayed in fig. 2 of FG08a are then

Table 2. Instrumental resolution [full width at half-maximum (FWHM)], pixel sizes and S/N properties adopted for the synthetic Lyα forest spectra. The values are based on those reported by FG08a.

Instrument	FWHM	Pixel size	S/N pixel^{-1}
HIRES	6 km s^{-1}	2 km s^{-1}	30
ESI	33 km s^{-1}	11 km s^{-1}	30
MIKE	11 km s^{-1}	2 km s^{-1}	20

drawn from our simulated data set in intervals of $\Delta z = 0.2$ between $2 \leq z \leq 4$.

The results are displayed as the open diamonds in Fig. 4 for the S1 (left-hand panel), E1 (central panel) and N1 (right-hand panel) models. Following FG08a, the error bars (statistical only) correspond to the standard error of the mean, computed by subdividing the synthetic data into chunks 3 proper Mpc in length. The solid curves in each panel correspond to the underlying $\tau_{\rm eff}$ evolution measured from the unprocessed synthetic Lyα spectra. Our results are compared to the best-fitting curve to the FG08a data, displayed by the dashed line in each panel.

As expected, the synthetic data in Fig. 4 now exhibit some additional scatter due to the variation in cosmic structure probed by the random sightlines, but in all instances are within 1σ of the underlying $\tau_{\rm eff}$ evolution. The S1 data in the left-hand panel again exhibit the generic behaviour seen in the semi-analytical model, and are inconsistent with the narrow feature observed by FG08a. For comparison, the central panel displays the data obtained from the E1 model with an extended period of heating (e.g. McQuinn et al. 2009), while the right-hand panel displays the N1 model with no additional heating from He II reionization. In both instances $\tau_{\rm eff}$ smoothly evolves with redshift. This result is in agreement with the predictions for $\tau_{\rm eff}$ from the radiative transfer simulations of McQuinn et al. (2009); an extended period of reheating during He II reionization will induce no sharp features in the $\tau_{\rm eff}$ evolution due to changes in the IGM temperature alone.

Our detailed simulations therefore indicate that hydrodynamical effects in the IGM following rapid reheating (but see Bolton et al. 2009; McQuinn et al. 2009) will not aid in reproducing the sharp dip in the Lyα opacity observed by FG08a. Instead, our results suggest any recovery in $\tau_{\rm eff}$ following sudden reheating will be driven primarily by adiabatic cooling in the low-density IGM, consistent with the behaviour predicted in our semi-analytical model.

6 HYDRODYNAMICS AND REDSHIFT-SPACE DISTORTIONS FOLLOWING SUDDEN REHEATING

In the last section we demonstrated our simulations were unable to reproduce the narrow feature observed by FG08a. We now consider this result in more detail by examining the impact of hydrodynamical effects and redshift-space distortions on the Lyα effective optical depth evolution.

6.1 The gas density distribution

We begin by briefly discussing the effect of sudden reheating on the IGM density distribution. Following an injection of energy into the IGM during reionization, the subsequent increase in gas pressure will smooth the IGM density distribution over scales corresponding to the local Jeans length (Schaye 2001; Pawlik, Schaye & van Scherpenzeel 2009). However, as noted by Gnedin & Hui (1998), this Jeans smoothing will not occur instantaneously. The low-density gas responsible for the Lyα forest absorption will expand on a sound-crossing time, which can be considerable – comparable to the Hubble time – in low-density systems. Indeed, hydrostatic equilibrium is only restored once $t_{\rm sc} \sim t_{\rm dyn}$, where $t_{\rm sc}$ and $t_{\rm dyn}$ are the sound crossing and dynamical time-scales, respectively (Schaye 2001). The dynamical time $t_{\rm dyn}$ in the low-density IGM is around the Hubble time, as is evident from the Friedmann equation, $H^2 = 8\pi G\rho$.

This can be appreciated in the comparison between sightline data drawn from the S1 (solid curves) and N1 (dotted curves) simulations displayed in Fig. 5. The left-hand panel displays a subsection of a single sightline through the simulations at $z = 3$, while the right-hand panel shows the same sightline at $z = 2$. From top to bottom, the normalized gas densities, the H I fractions, the gas temperatures, the peculiar velocities and the resulting Lyα forest spectra, computed in three different ways, are displayed. The spectra in the third row from bottom are computed using equation (5) and include the effect of redshift-space distortions due to the peculiar velocity field. In the next row down, however, the N1 spectrum has been recomputed by fixing the gas temperature in the N1 model to be equal to the S1 values and then rescaling the N1 H I fraction, such that $n'_{\rm H\,I} = n_{\rm H\,I}(T_{\rm S1}/T_{\rm N1})^{-0.7}$. This removes most of differences in the spectra attributable to Doppler broadening and the H I fraction, although note the $T^{-0.7}$ scaling for the recombination coefficient is not exact

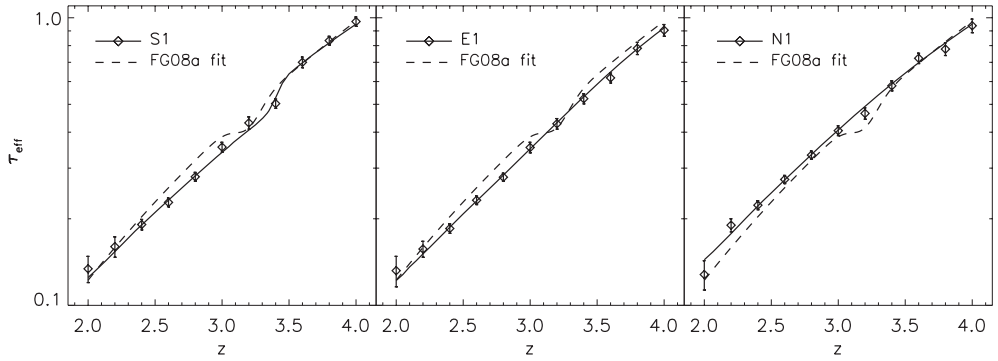

Figure 4. A comparison of the $\tau_{\rm eff}$ evolution measured from synthetic Lyα spectra drawn from three of our hydrodynamical simulations to the best-fitting curve from FG08a (dashed curves). The solid curves in each panel display $\tau_{\rm eff}$ measured from the unprocessed synthetic Lyα spectra, while the open diamonds with error bars correspond to $\tau_{\rm eff}$ measured in bins of width $\Delta z = 0.2$ after the spectra are processed to closely resemble the FG08a data set. The error bars correspond to the standard error of the mean. Left: the S1 model. Centre: the E1 model. Right: the N1 model.

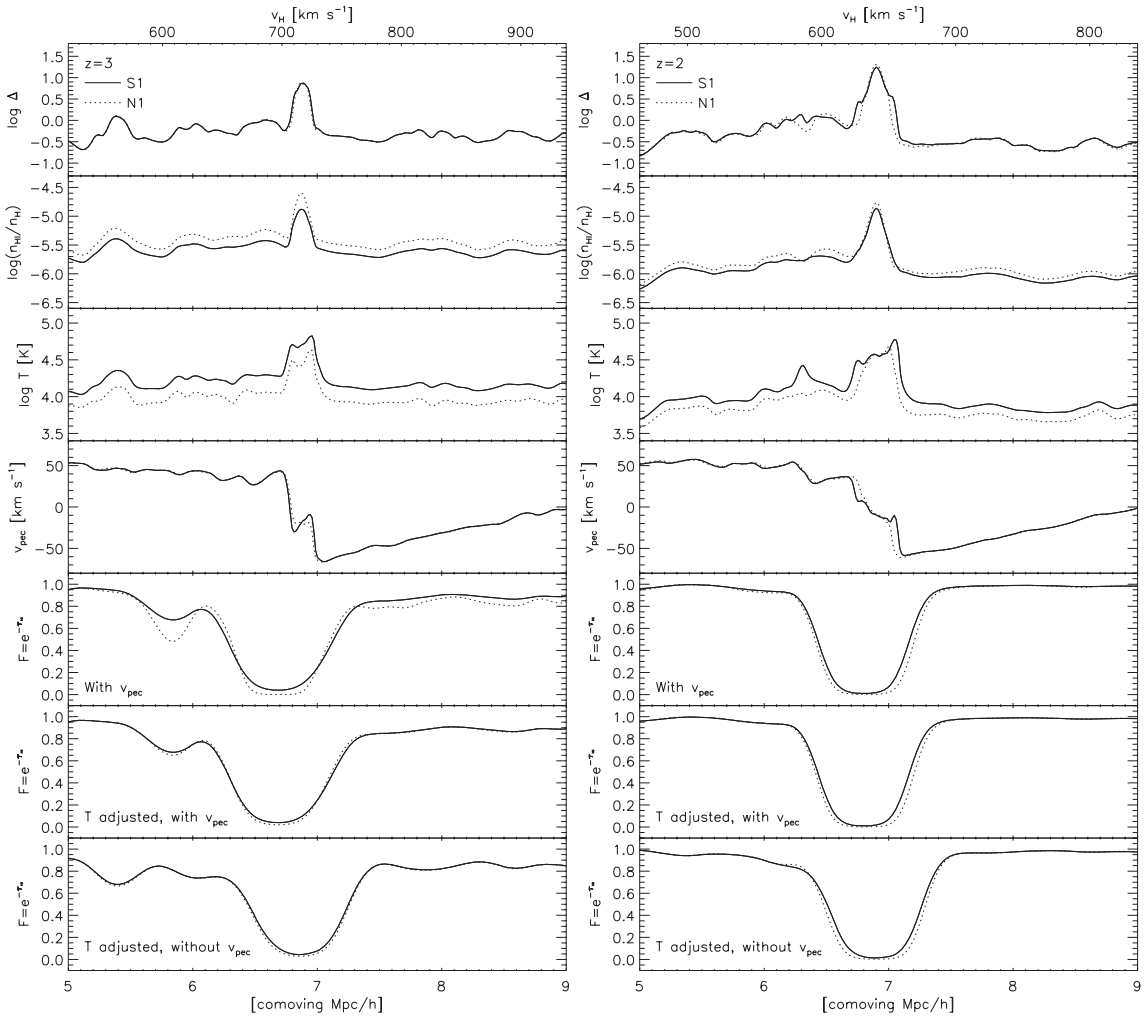

Figure 5. Comparison between various IGM properties along a subsection of a sightline extracted from identical locations in the S1 (solid curves) and N1 simulations (dotted curves) at $z = 3$ (left-hand panel) and $z = 2$ (right-hand panel). From top to bottom, the normalized gas densities, the H I fractions, the gas temperatures, the peculiar velocities and the resulting Lyα forest spectra, computed in three different ways, are displayed. The spectra in the third row from bottom are computed using equation (5) and include the effect of the peculiar velocity field. In the next row, however, the N1 spectrum has been recomputed by fixing the gas temperature in the N1 model to be equal to the S1 values and then rescaling the N1 H I fraction, such that $n'_{\rm H\,I} = n_{\rm H\,I}(T_{\rm S1}/T_{\rm N1})^{-0.7}$. This removes most of differences in the spectra attributable to Doppler broadening and the H I fraction. The S1 and temperature adjusted N1 spectra both exclude the effect of the peculiar velocity field in the bottom row.

and small differences will remain.[4] Finally, in the bottom row the S1 and temperature adjusted N1 spectra both exclude the effect of the peculiar velocity field.

It is clear that differences in the Lyα spectra due to the gas density alone are very small soon after reheating. The density distribution at $z = 3$ has only been slightly smoothed around the peak of the overdensity located at $6.9\,h^{-1}$ Mpc. In contrast, pressure smoothing of the gas distribution is clearly apparent by $z = 2$, as there has been sufficient time for the gas distribution to be altered by the increased pressure in the high-density regions. It is precisely because of the finite time-scale required to achieve hydrostatic equilibrium that changes in the gas density distribution due to Jeans smoothing will have a negligible impact on the $\tau_{\rm eff}$ evolution by $z = 3$ if the IGM is suddenly heated at $z = 3.4$.

6.2 Peculiar velocity gradients

However, the finite time required to change the gas distribution does not exclude rapid changes in the peculiar velocity *gradients* responsible for the Jeans smoothing. Redshift-space distortions associated with these gradients may then induce changes in the Lyα line profiles (Bryan et al. 1999; Theuns, Schaye & Haehnelt 2000). T02 appealed to these peculiar velocity gradients to explain the recovery in the $\tau_{\rm eff}$ feature observed by Bernardi et al. (2003). On examination of the peculiar velocity field in the left-hand panel of Fig. 5, the S1 model does indeed exhibit a positive peculiar velocity gradient in the centre of the overdensity at $6.9\,h^{-1}$ Mpc, as it must if the gas is to expand. The increased gas pressure has reversed the collapse of the overdensity which is occurring in the colder N1 model.

[4] In the left-hand panel of Fig. 5 prior to this rescaling, the larger difference between the S1 and N1 line profiles at $5.8\,h^{-1}$ Mpc on comparison to the broader lines at $6.7\,h^{-1}$ Mpc is because these absorption features lie on the linear and logarithmic parts of the curve of growth, respectively.

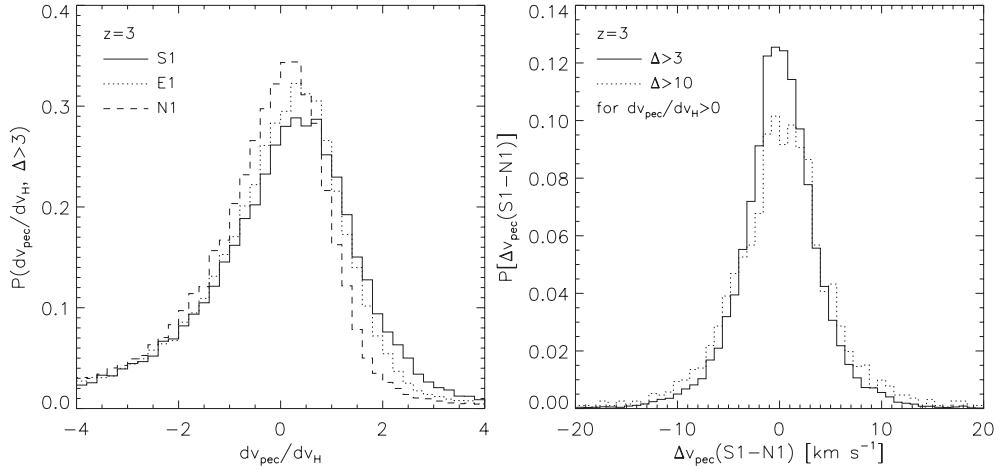

Figure 6. Left: probability distribution of the peculiar velocity derivative with respect to the Hubble velocity, $v_{\rm H}$, in the S1 (solid curve), E1 (dotted curve) and N1 (dashed curve) simulations at $z = 3$. The probability distribution is for gas with $\Delta > 3$ only. The shift in the probability distribution towards more positive gradients for progressively hotter models is associated with expansion in the higher density regions in the simulations. Right: the probability distribution function of the *difference* between the peculiar velocity fields in the S1 and N1 models in all regions where there is a positive velocity gradient in the S1 model (i.e. regions which are expanding). The solid and dotted curves display the distributions for all gas with $\Delta > 3$ and >10, respectively. The largest values of $\Delta v_{\rm pec}$ correspond to the densest regions in the simulations.

This effect of gas temperature on the peculiar velocity gradients is displayed in more detail in the left-hand panel of Fig. 6, where the probability distribution of the peculiar velocity derivative with respect to the Hubble velocity, $\mathrm{d}v_{\rm pec}/\mathrm{d}v_{\rm H}$, in all 1024 synthetic sightlines is shown for the S1 (solid curve), E1 (dotted curve) and N1 (dashed curve) simulations. The distribution is shown for overdense gas with $\Delta > 3$ only (cf. fig. 3 in Theuns et al. 2000). The shift in the probability distribution towards more positive gradients for progressively hotter models is due to expansion in the hotter, high-density regions which have become overpressurized with respect to their cooler surroundings (Bryan et al. 1999; Theuns et al. 2000). The fact that the probability distributions look qualitatively similar to the data presented in fig. 3 of Theuns et al. (2000) is encouraging, and indicates the higher temperatures in our GADGET-2 simulations have a similar impact on the peculiar velocity field. Theuns et al. (2000) used simulations performed with HYDRA in a $2.5\,h^{-1}$ comoving Mpc box with a gas particle masses of $1.14 \times 10^6\,{\rm M}_\odot$ (similar to our mass resolution). Note the larger velocity gradients present in our simulations are most likely due to the additional large-scale power present in our significantly bigger simulation boxes ($15\,h^{-1}$ comoving Mpc).

In the example sightline in Fig. 5, the maximum difference between the peculiar velocities in the S1 and N1 models is $\sim$10 km s^{-1} in the centre of the overdensity. Although this difference indeed has some impact on the line profile, the change in the peculiar velocity field is small on comparison to the linewidth, and it is not enough to significantly alter the broad Lyα line shown in the lower panels. Once differences attributable to the different temperatures of the simulations have been scaled out of the spectra, the S1 and N1 models produce very similar absorption line profiles.

This anecdotal evidence is displayed more quantitatively in the right-hand panel of Fig. 6, where we plot the probability distribution of the *difference* between the peculiar velocities in the S1 and N1 simulations for all pixels with positive peculiar velocity gradients and $\Delta > 3$ (solid curve) or $\Delta > 10$ (dotted curve) in the S1 data. In the majority of these regions there is in fact only a small change in the peculiar velocity field, with the largest differences ($\sim 10\,{\rm km\,s^{-1}}$) associated with the rarer, high-density peaks which produce broad lines like the one shown in Fig. 5. Since an absolute change in the peculiar velocity of a few km s^{-1} is small in comparison to typical linewidths of 20 km s^{-1} (e.g. Kim et al. 2002), this explains why the impact on $\tau_{\rm eff}$ is correspondingly small. Instead, it is the *instantaneous* temperature of the IGM which primarily influences the $\tau_{\rm eff}$ evolution in our simulations.

These findings differ from those of T02, who found changes in the peculiar velocity gradients were partially responsible for inducing the recovery in $\tau_{\rm eff}$ observed by Bernardi et al. (2003). The discrepancy between these results may be due to differences between the numerical methods used. We have tested the impact of time-stepping on simulations, and we find our results are robust in this respect. However, we cannot be absolutely certain that other numerical effects do not play a role, and ultimately we can only speculate on the origin of this difference. Ideally, an independent numerical study is required to verify or refute our claims. In agreement with T02, however, we do indeed find that line blending due to the peculiar velocity field lowers $\tau_{\rm eff}$, and that higher temperatures steepen the peculiar velocity gradients in overdense regions, giving us confidence that our simulations are at least broadly consistent with T02. We find these effects are nevertheless insufficient to reproduce the narrow feature observed in the $\tau_{\rm eff}$ evolution, suggesting that a sudden increase in the IGM temperature at $z = 3.4$ following He II reionization is unable to adequately explain the $\tau_{\rm eff}$ data.

7 ON THE POSSIBLE ORIGIN OF THE OBSERVED $\tau_{\rm eff}$ FEATURE

Thus far we have established that even in the presence of a sudden increase in the IGM temperature at $z = 3.4$ (but see Bolton et al. 2009; McQuinn et al. 2009), the narrow dip observed in the Lyα effective optical depth by FG08a cannot be reproduced in our hydrodynamical simulations of the Lyα forest. However, before proceeding it is worth briefly emphasizing that the purported 'narrowness' of the $\tau_{\rm eff}$ feature is a somewhat model-dependent statement. For instance, if we consider the $\tau_{\rm eff}$–z plane, FG08a characterized the width of the feature by fitting a power law and a Gaussian 'bump'. This

significance of the bump then depends on how good an approximation a power law is to the underlying evolution of the IGM opacity excluding the effects associated with He II reionization. In our simulations without sudden heating, $\tau_{\rm eff}$ does indeed evolve smoothly with redshift, indicating this should be a reasonable approximation if the redshift evolution of the ionizing background is gradual. In contrast, the FG08a feature stands out visually, and more objective measures we have applied to the data (e.g. a regularized derivative of the data as used in edge-finding algorithms) tend to confirm that impression. The fact that it is seen in at least three independent data sets further hints that it is not a data artefact.

Additionally, a decomposition into the required evolution in the ionizing background (as in the next section) will also depend on the assumed IGM thermal evolution. The Lyα opacity scales as $\tau \propto T^{-0.7}/\Gamma_{\rm H\,I}$; the effect of gas temperature and the photoionization rate on $\tau_{\rm eff}$ are impossible to disentangle without independent estimates for one or the other. In this work we have demonstrated that sudden heating on its own cannot reproduce the $\tau_{\rm eff}$ feature. However, a sudden global heating event followed by a gradual downturn in the photoionization rate at $z < 3.2$ could still reproduce the data. On the other hand, there is good reason to suppose that such a sudden, global boost to the IGM temperature is unlikely in the first place. Our previous work has demonstrated that He II reionization likely produces too little heating to produce a substantial opacity decrease over the short time-scale required (Bolton et al. 2009). In the next section we therefore assume the temperature boost during He II reionization occurs over an extended period of time (our E1 model). This model also resembles the results from recent radiative transfer simulations performed by McQuinn et al. (2009). We therefore dispense with rapid changes in the temperature entirely, and now turn to discuss the remaining possibility for the origin of the $\tau_{\rm eff}$ dip: a narrow peak in the metagalactic hydrogen photoionization rate.

7.1 The hydrogen photoionization rate required by the FG08a $\tau_{\rm eff}$ evolution

Many studies have used simulations of the Lyα forest, combined with measurements of $\tau_{\rm eff}$, to place constraints on the metagalactic hydrogen photoionization rate, $\Gamma_{-12} = \Gamma_{\rm H\,I}/10^{-12}\,{\rm s}^{-1}$ (e.g. Rauch et al. 1997; McDonald & Miralda-Escudé 2001; Cen & McDonald 2002; Schaye et al. 2003; Meiksin & White 2004; Tytler et al. 2004; Bolton et al. 2005; Jena et al. 2005). We use the same procedure in this work to estimate Γ_{-12} from our E1 simulation, which was constructed to have a similar thermal history at mean density to the recent radiative transfer simulations of McQuinn et al. (2009). We use equation (7) and the best fit[5] to $\tau_{\rm eff}$ obtained by FG08a for this purpose. Following from equation (2), the photoionization rate which reproduces the $\tau_{\rm eff}$ fit is given by $\Gamma_{-12}(z) = \Gamma_{\rm HM}(z)/A(z)$, where $\Gamma_{\rm HM}(z)$ is the photoionization rate from the HM01 UVB model divided by $10^{-12}\,{\rm s}^{-1}$.

The result of this procedure is displayed as the solid curve in Fig. 7. A gradual increase in Γ_{-12} towards lower redshift is required, and the prominent bump centred at $z = 3.2$ is responsible for the narrow $\tau_{\rm eff}$ feature. The open diamonds with error bars are derived from the FG08a $\tau_{\rm eff}$ data points including their 1σ statistical errors; these give an indication of the statistical uncertainty in this peak.

[5] Specifically, we use the best fit FG08a present for their $\tau_{\rm eff}$ measurements in redshift bins of width $\Delta z = 0.2$ when using the Schaye et al. (2003) metal correction.

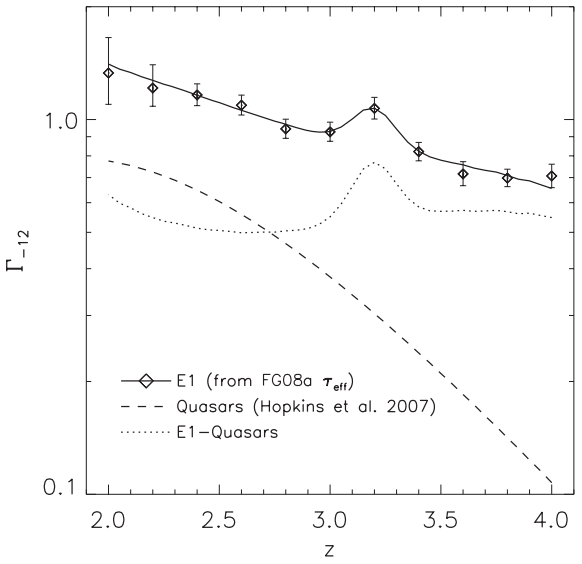

Figure 7. The solid curve corresponds to the hydrogen photoionization rate, $\Gamma_{-12} = \Gamma_{\rm H\,I}/10^{-12}\,{\rm s}^{-1}$, required to reproduce the fit to $\tau_{\rm eff}$ evolution presented by FG08a. The narrow peak in Γ_{-12} at $z = 3.2$ corresponds to the dip in the FG08a $\tau_{\rm eff}$ evolution. The dashed curve displays the expected contribution of quasars to the total Γ_{-12}, based on the Hopkins et al. (2007) model for the quasar luminosity function, and the dotted line corresponds to the difference between the total Γ_{-12} required by $\tau_{\rm eff}$ and the quasar only contribution. To give an indication of the statistical uncertainty in this peak, the open diamonds with error bars are derived from the FG08a $\tau_{\rm eff}$ data points including their 1σ statistical errors.

The dashed curve shows the expected contribution from quasars to Γ_{-12}. We compute this using the recent Madau & Haardt (2009) parametrization for the Hopkins et al. (2007) comoving quasar emissivity at the H I Lyman limit, $\nu_{\rm L}$, assuming a power-law spectrum with $\epsilon_\nu^{\rm Q} = \epsilon_{\rm L}(\nu/\nu_{\rm L})^{-1.6}$ (e.g. Telfer et al. 2002). The expected contribution to the photoionization rate from quasars is then

$$\Gamma_{-12}^{\rm Q} = \frac{(1+z)^3}{10^{-12}\,{\rm s}^{-1}} \int_{\nu_{\rm L}}^{\infty} \frac{\epsilon_\nu^{\rm Q} \lambda_\nu \sigma_\nu}{h_{\rm p}\nu}\,{\rm d}\nu, \qquad (9)$$

where the photoionization cross-section $\sigma_\nu = 6.3 \times 10^{-18}\,{\rm cm}^2\,(\nu/\nu_{\rm L})^{-3}$ and the mean free path $\lambda_\nu = \lambda_{\rm L}(\nu/\nu_{\rm L})^{1.5}$; the latter assumes the H I column density distribution $f(N_{\rm H\,I}, z) \propto N_{\rm H\,I}^{-1.5}$ (e.g. Petitjean et al. 1993; Miralda-Escudé 2003). We take $\lambda_{\rm L} = 50[(1+z)/4]^{-4}$ proper Mpc, which is towards the lower end of the range recently advocated by Faucher-Giguère et al. (2008b). Note, however, that the expected contribution to the photoionization rate from quasars depends on the uncertain quasar luminosity function (particularly the faint end slope), mean free path and ionizing spectrum, as well as radiative transfer effects (for instance, reprocessed radiation can contribute significantly; Haardt & Madau 1996).

The dotted curve displays the difference between the total photoionization rate and the contribution from quasars alone, $\Gamma'_{-12} = \Gamma_{-12} - \Gamma_{-12}^{\rm Q}$. This curve remains almost flat for $2 \leq z \leq 4$, with $\Gamma'_{-12} \simeq 0.55$, aside from the narrow bump ($\Delta z \simeq 0.4$) which peaks with $\Gamma'_{-12} \simeq 0.75$ at $z = 3.2$. Thus, in order to reproduce the observed $\tau_{\rm eff}$, we require a boost of around 35–40 per cent in Γ'_{-12} over a short redshift interval.

Finally, note that although the FG08a statistical errors are relatively small, the normalization of Γ_{-12} is still somewhat uncertain. In particular, although the Γ_{-12} values we derive from our E1 simulation are consistent with other estimates from hydrodynamical simulations (Tytler et al. 2004; Bolton et al. 2005; Jena et al. 2005),

they are systematically higher by up to a factor of 2 in comparison to the recent estimates presented by Faucher-Giguère et al. (2008b) using the same $\tau_{\rm eff}$ data. This is partially because Faucher-Giguère et al. (2008b) do not model the Lyα forest in detail, instead obtaining analytical estimates for Γ_{-12} using the FGPA combined with the IGM density distribution derived by Miralda-Escudé et al. (2000) (see equations 2 and 3). Systematic uncertainties on Γ_{-12} due to other parameters, such as the IGM temperature which is still poorly constrained, are also large (Bolton et al. 2005). Thus, although the overall normalization remains somewhat uncertain, the *shape* of these curves should be fairly robust, and the requirement for a peak in Γ_{-12} remains so long as the volume weighted IGM temperature evolves slowly (McQuinn et al. 2009).

7.2 Possible causes of a peak in the hydrogen photoionization rate

We have found that, even if the IGM temperature increases suddenly, we cannot reproduce a narrow feature in the optical depth.[6] Thus a narrow peak at $z = 3.2$ in the otherwise approximately constant value of $\Gamma'_{-12} = \Gamma_{-12} - \Gamma^{\rm Q}_{-12}$ from $2 \leq z \leq 4$ is instead required to reproduce the $\tau_{\rm eff}$ evolution measured by FG08a. This could be associated with a sharp modulation in the ionizing emissivity or the mean free path of ionizing photons, or indeed a combination of both effects (see equation 9). However, while appealing to the stellar contribution to the photoionization rate for an increase in the emissivity is in principle acceptable given the uncertainties involved in deriving the stellar ionizing rate from observations at $z > 3$ (e.g. Madau, Haardt & Rees 1999; Miralda-Escudé 2003; Bolton & Haehnelt 2007b), there is no apparent reason why such a narrow peak should occur at $z = 3.2$.

Instead, we suggest it is more likely that any modulation of the hydrogen photoionization rate is associated with dense He II and H I Lyman limit systems (LLSs). Unlike the low-density IGM, such systems have dynamical, cooling and recombination times which are comparable or shorter than the $\sim 10^8$ yr associated with the width of the $\tau_{\rm eff}$ feature. They can modulate the hydrogen ionizing background, either by changing the hydrogen ionizing emissivity (by the reprocessing of He II ionizing photons into He II Lyman series, Balmer or two-photon emission, all of which can ionize hydrogen), or the mean free path of ionizing photons, since their opacity will be altered by changes in their size or temperature.[7] Furthermore, a sharp change in the emissivity or opacity will then be imprinted on the ionizing background on a time-scale comparable to the mean free time of an ionizing photon, or $\Delta z \sim ({\rm d}N/{\rm d}z)^{-1}$ $[\Gamma(\beta - 1)]^{-1} \sim 0.24$ where ${\rm d}N/{\rm d}z = 3.3\,[(1+z)/5]^{1.5}$ is the abundance of H I LLSs (Storrie-Lombardi et al. 1994), and we assume ${\rm d}N/{\rm d}N_{\rm H\,I} \propto N_{\rm H\,I}^{-\beta}$ with $\beta = 1.5$. This is certainly well within the range required to explain the feature. We now proceed to give some brief examples of these effects.

(i) *Helium recombination radiation*

A large fraction of the hydrogen ionizing background may be radiation from higher frequencies that is reprocessed by dense systems. For instance, Haardt & Madau (1996) find that $\sim$40 per cent of $\Gamma_{\rm H\,I}$ comes from reprocessed radiation at $z \sim 3$; similarly Fardal, Giroux & Shull (1998) find that about $\sim$20 per cent of $\Gamma_{\rm H\,I}$ comes from reprocessed radiation. This has two components: recombinations of hydrogen to the ground state, and reprocessing of He II ionizing photons into He II Lyman series, Balmer or two-photon emission, all of which can ionize hydrogen. The latter obviously undergoes rapid evolution during the process of He II reionization, particularly toward the tail end of reionization when the mean ionizing background can rise rapidly (although there could be large fluctuations in the background throughout the reionization process; Furlanetto 2008). On the other hand, recent calculations indicate the contribution of recombination radiation to the UVB could be smaller than previous estimates (Faucher-Giguère et al. 2009).

Another potentially important effect comes from the reprocessing of He II Lyman series photons in an optically thick IGM (Madau & Haardt 2009). Lyman series photons between Lyβ (at $E = 3.56$ Ry) and the Lyman limit (4 Ry) are degraded to He II Lyα photons, Balmer or lower frequency radiation. The magnitude of this effect depends strongly on the opacity of the IGM, which of course evolves rapidly during He II reionization. While this may not appear to be particularly significant (since such photons can already ionize hydrogen), the degradation to lower energies implies that the hydrogen photoionization rate can be significantly modulated. In particular, selection rules forbid Lyβ photons from being converted into Lyα photons, and the reduction of two-photon emission from Lyβ reprocessing at the end of He II reionization could reduce the hydrogen ionization rate, helping to produce the downturn in the photoionization rate.

(ii) *The size of LLSs*

In this work, we have thus far argued that hydrodynamic effects associated with the heating of the IGM during He II reionization have little effect on $\tau_{\rm eff}$. While this is true of the low-density gas responsible for most of the absorption in the Lyα forest, it is not true of higher density systems which have smaller dynamical timescales, $t_{\rm dyn} \propto \Delta^{-1/2}$. Since H I LLSs dominate the opacity of the post-reionization IGM, a sudden change in the sizes of these systems can then modulate the mean free path of H I ionizing photons.

We may consider this as follows. At the end of He II reionization, although most of the IGM has been reheated, self-shielded He II LLSs, in which the helium is still predominantly in the form of He II, will still remain. Self-shielding to He II ionizing photons occurs for He II column densities $N_{\rm He\,II} > 6.7 \times 10^{17}\,{\rm cm}^{-2}$. Assuming the size of an absorber with overdensity $\Delta$is the local Jeans length (Schaye 2001), this column density corresponds to a characteristic overdensity

$$\Delta \simeq 56 \left(\frac{T}{10^4\,{\rm K}}\right)^{2/15} \left(\frac{1+z}{4}\right)^{-3} \Gamma_{-14}^{2/3}, \qquad (10)$$

where $\Gamma_{-14} = \Gamma_{\rm He\,II}/10^{-14}\,{\rm s}^{-1}$ is the He II photoionization rate. The H I column density of an absorber with overdensity $\Delta$is (Schaye 2001)

$$N_{\rm H\,I} \simeq 3.8 \times 10^{16}\,{\rm cm}^{-2}\,\frac{\Delta^{3/2}}{\Gamma_{-12}} \left(\frac{T}{10^4\,{\rm K}}\right)^{-1/5} \left(\frac{1+z}{4}\right)^{9/2}. \qquad (11)$$

Self-shielding to He II ionizing photons therefore happens at an H I column density of $N_{\rm H\,I} \sim 1.6 \times 10^{16}\,{\rm cm}^{-2}$ $(\Gamma_{-14}/\Gamma_{-12})$, well short of the column density of $N_{\rm H\,I} \sim 1.6 \times 10^{17}\,{\rm cm}^{-2}$ associated with H I LLSs. Thus, at face value it may seem that He II reionization cannot substantially affect H I LLSs, and hence the mean free path of H I ionizing photons. However, He II LLSs are also likely to be associated with the less dense outer regions of H I LLSs. A strong increase in external pressure due to the reheating of the IGM during

[6] The exception to this is if the photoionization rate subsequently drops at $z < 3.2$ following a sudden temperature increase. However, as discussed earlier, recent studies indicate that a rapid global temperature boost is unlikely in the first place (Bolton et al. 2009; McQuinn et al. 2009).

[7] The heating and expansion of LLSs was also briefly discussed by McQuinn et al. (2009).

He II reionization then means that the system will no longer be in hydrostatic equilibrium. The pressure gradient compresses the gas,[8] until pressure equilibrium is once again restored (a similar mechanism has been invoked for globular cluster formation; e.g. Cen 2001). As a result, H I LLSs could decrease in size, and increase in density. Alternatively, if hard photons can penetrate and heat the gas in the high-density regions (e.g. Bolton et al. 2009), the H I LLS could instead expand.

For simplicity, let us for the moment assume that any change in density occurs isothermally (see below for more discussion). If the absorber expands or contracts to a new overdensity $\Delta \rightarrow f\Delta$, then (since $n_{\rm H\,I} \propto \Delta^2$ and $R \propto \Delta^{-1/3}$), $N_{\rm H\,I} \propto f^{5/3}$, while the cross-section of the absorber $\sigma \propto f^{-2/3}$. Assuming that f is independent of Δ(the opacity is dominated by H I LLSs, so the result will be most affected by f for such systems), the mean free path of ionizing photons will be altered by a factor

$$\frac{\lambda}{\lambda_{\rm L}} = \frac{\int_{0.1}^{\infty} \tau^{-1.5} \left[1 - \exp(-\tau)\,{\rm d}\tau\right]}{\int_{0.1}^{\infty} f^{-2/3}\tau^{-1.5} \left[1 - \exp(-f^{5/3}\tau)\,{\rm d}\tau\right]}, \quad (12)$$

where the lower limit $\tau \sim 0.1$ is the H I optical depth at which systems self-shield from He II ionizing radiation. This is a non-monotonic function with a minimum at $f \sim 0.3$; however, it does not exceed unity until $f > 1$. Thus, if systems compress, the hydrogen photoionization rate falls; if they expand, it increases. However, more quantitative exploration of this possibility requires careful simulation of the LLS with coupled hydrodynamics and radiative transfer, particularly since the equilibrium temperature also strongly affects opacity. In addition, a caveat to this argument is that although the dynamical time-scale of an individual LLS is comparable to that required for the modulation of $\Gamma_{\rm H\,I}$, a globally averaged change in the mean free path still requires the size of all the LLSs to change over a short time interval.

(iii) *The temperature of LLSs*

Yet another possibility is that the temperature of H I LLSs itself changes during He II reionization, altering their opacity. A rapid increase in the injection of photons at 3 Ry from reprocessed radiation implies that the ionizing background hardens significantly, which could result in a significant change in the equilibrium temperature. This could be further modulated by the hydrodynamic effects mentioned above. Note that the equilibrium temperature of LLSs is a non-trivial function of density in photoionization equilibrium, particularly in the presence of metal line cooling (Wiersma, Schaye & Smith 2009). Generally, as a system becomes denser, the equilibrium temperature falls, since the efficiency of cooling increases as the ionization parameter falls (Efstathiou 1992; Wiersma et al. 2009). This exacerbates the increase in opacity due to the density increase. Non-monotonic evolution of the temperature of the LLSs (which have short cooling times since they cool radiatively, rather than adiabatically) could thus modulate their opacity, as well as the mean free path and the H I photoionization rate.

8 CONCLUSIONS

We have used a semi-analytic model of inhomogeneous He II reionization and high-resolution hydrodynamical simulations of the Lyα forest to investigate the impact of sudden reheating on the evolution of the Lyα forest effective optical depth. Our semi-analytic model indicates that any injection of energy into the IGM during inhomogeneous He II reionization will produce a well-understood and generic evolution in $\tau_{\rm eff}$, where a reduction in the opacity from $z = 4$ to 3 is followed by a gradual, monotonic recovery driven largely by adiabatic cooling in the low-density IGM. This behaviour is inconsistent with the narrow dip ($\Delta z = 0.4$) of around 10 per cent in $\tau_{\rm eff}$ at $z = 3.2$ which has now been detected by three independent observational studies (Bernardi et al. 2003; Dall'Aglio et al. 2008; FG08a).

However, our semi-analytic model does not include a detailed reconstruction of the Lyα forest. We therefore also analyse five high-resolution hydrodynamical simulations of the IGM to investigate the effect of various thermal histories on the Lyα effective optical depth. We find that sudden reheating at $z = 3.4$ results in a sharp decrease in $\tau_{\rm eff}$, although we note that such a large, sudden increase in the IGM temperature is nevertheless unlikely to occur over the entire IGM at once (Bolton et al. 2009; McQuinn et al. 2009). This assumption may nevertheless be appropriate in localized regions around quasars with hard spectra, and in small volumes similar to the box size of our hydrodynamical simulations.

Although the assumption of sudden, homogeneous reheating does indeed successfully reproduce the initiation of the $\tau_{\rm eff}$ dip observed by FG08a, our simulations are still unable to account for the rapid *recovery* of the narrow dip in the $\tau_{\rm eff}$ evolution by $z = 2.9$. The effect of the 8 per cent increase in the free extra fraction following He II reionization on $\tau_{\rm eff}$ is small, and any resulting increase in $\tau_{\rm eff}$ is instead countered by the simultaneous flattening of the power-law temperature–density relation during instantaneous, homogeneous He II reionization at $z = 3.4$. Redshift-space distortions in the Lyα forest attributable to the response of the gas to the extra energy injected into the IGM are also unable to account for the observed recovery of $\tau_{\rm eff}$. We find that sudden reheating does indeed produce larger, more positive peculiar velocity gradients corresponding to regions of newly expanding gas, but the absolute changes in the velocity field are generally small in comparison to typical linewidths, except in the most overdense regions in the simulation. Such regions are, however, rare and thus contribute little to the average opacity. We have tested the robustness of this result with respect to the time integration scheme employed in GADGET-2, and we find this has little impact on our numerical results. In contrast, if He II reionization is an extended process, then in agreement with the recent study by McQuinn et al. (2009) we find the Lyα effective optical depth will evolve smoothly with redshift.

As a consequence, we must instead appeal to a narrow peak in the metagalactic hydrogen photoionization rate at $z = 3.2$ to reproduce the $\tau_{\rm eff}$ feature in our simulations. This could potentially be modulated by LLSs, which have recombination, cooling and dynamical times comparable to or less than the time-scale associated with the width of the feature. In particular, we suggest that radiative transfer effects from He II reionization itself could be responsible, either by altering the emissivity of reprocessed He II recombination photons, or by changing the opacity of H I LLSs and hence the mean free path of ionizing photons. However, further detailed investigation is still required to establish the origin of this intriguing feature in the redshift evolution of the Lyα forest opacity.

ACKNOWLEDGMENTS

We thank George Becker, Claude-André Faucher-Giguère, Martin Haehnelt, Joop Schaye, Tom Theuns and Matteo Viel for helpful discussions during the course of this work. We are also very grateful to Volker Springel for his advice and for providing GADGET-2. The

[8] Note that in our optically thin hydrodynamical simulations the self-shielding of dense systems is not modelled. This effect is therefore absent in our simulation data.

hydrodynamical simulations used in this work were performed using the SGI Altix 4700 supercomputer COSMOS at the Department of Applied Mathematics and Theoretical Physics in Cambridge. COSMOS is a UK-CCC facility which is sponsored by SGI, Intel, HEFCE and STFC. This research was also supported in part by the National Science Foundation under Grant Nos. PHY05-51164 (JSB, through the MPA/KITP post-doctoral exchange programme), AST-0829737 (SRF), the David and Lucile Packard Foundation (SRF) and NASA grant NNG06GH95G (SPO). JSB thanks the staff at the Kavli Institute for Theoretical Physics, Santa Barbara, for their hospitality during the early stages of this work.

REFERENCES

Abel T., Haehnelt M. G., 1999, ApJ, 520, L13
Becker G. D., Rauch M., Sargent W. L. W., 2007, ApJ, 662, 72
Bernardi M. et al., 2003, AJ, 125, 32
Bi H. G., Boerner G., Chu Y., 1992, A&A, 266, 1
Bolton J. S., Haehnelt M. G., 2007a, MNRAS, 374, 493
Bolton J. S., Haehnelt M. G., 2007b, MNRAS, 382, 325
Bolton J., Meiksin A., White M., 2004, MNRAS, 348, L43
Bolton J. S., Haehnelt M. G., Viel M., Springel V., 2005, MNRAS, 357, 1178
Bolton J. S., Viel M., Kim T.-S., Haehnelt M. G., Carswell R. F., 2008, MNRAS, 386, 1131
Bolton J. S., Oh S. P., Furlanetto S. R., 2009, MNRAS, 395, 736
Bryan G. L., Machacek M., Anninos P., Norman M. L., 1999, ApJ, 517, 13
Cen R., 2001, ApJ, 560, 592
Cen R., McDonald P., 2002, ApJ, 570, 457
Couchman H. M. P., Thomas P. A., Pearce F. R., 1995, ApJ, 452, 797
Dall'Aglio A., Wisotzki L., Worseck G., 2008, A&A, 491, 465
Davidsen A. F., Kriss G. A., Wei Z., 1996, Nat, 380, 47
Dunkley J. et al., 2009, ApJS, 180, 306
Efstathiou G., 1992, MNRAS, 256, 43
Eisenstein D. J., Hu W., 1999, ApJ, 511, 5
Fardal M. A., Giroux M. L., Shull J. M., 1998, AJ, 115, 2206
Faucher-Giguère C.-A., Prochaska J. X., Lidz A., Hernquist L., Zaldarriaga M., 2008a, ApJ, 681, 831 (FG08a)
Faucher-Giguère C.-A., Lidz A., Hernquist L., Zaldarriaga M., 2008b, ApJ, 688, 85
Faucher-Giguère C.-A., Lidz A., Zaldarriaga M., Hernquist L. 2009, ApJ, submitted (arXiv:0901.4554)
Fechner C. et al., 2006, A&A, 455, 91
Furlanetto S. 2008, ApJ, submitted (arXiv:0812.3411)
Furlanetto S. R., Oh S. P., 2008a, ApJ, 681, 1
Furlanetto S. R., Oh S. P., 2008b, ApJ, 682, 14
Gnedin N. Y., Hui L., 1998, MNRAS, 296, 44
Gunn J. E., Peterson B. A., 1965, ApJ, 142, 1633
Haardt F., Madau P., 1996, ApJ, 461, 20
Haardt F., Madau P., 2001, in Neumann D. M., Tran J. T. V., eds, Clusters of Galaxies and the High Redshift Universe Observed in X-rays, preprint (astro-ph/0106018) (HM01)
Haehnelt M. G., Steinmetz M., 1998, MNRAS, 298, L21
Heap S. R., Williger G. M., Smette A., Hubeny I., Sahu M. S., Jenkins E. B., Tripp T. M., Winkler J. N., 2000, ApJ, 534, 69
Hernquist L., Katz N., Weinberg D. H., Miralda-Escudé J., 1996, ApJ, 457, L51
Hjerting F., 1938, ApJ, 88, 508
Hopkins P. F., Richards G. T., Hernquist L., 2007, ApJ, 654, 731
Hui L., Gnedin N. Y., 1997, MNRAS, 292, 27
Hui L., Haiman Z., 2003, ApJ, 596, 9
Jakobsen P., Boksenberg A., Deharveng J. M., Greenfield P., Jedrzejewski R., Paresce F., 1994, Nat, 370, 35
Jena T. et al., 2005, MNRAS, 361, 70
Kim T.-S., Carswell R. F., Cristiani S., D'Odorico S., Giallongo E., 2002, MNRAS, 335, 555
McDonald P., Miralda-Escudé J., 2001, ApJ, 549, L11
McDonald P., Miralda-Escudé J., Rauch M., Sargent W. L. W., Barlow T. A., Cen R., 2001, ApJ, 562, 52
McQuinn M., Lidz A., Zaldarriaga M., Hernquist L., Hopkins P. F., Dutta S., Faucher-Giguere C. A., 2009, ApJ, 694, 842
Madau P., Haardt F., 2009, ApJ, 693, L100
Madau P., Haardt F., Rees M. J., 1999, ApJ, 514, 648
Maselli A., Ferrara A., 2005, MNRAS, 364, 1429
Meiksin A., White M., 2004, MNRAS, 350, 1107
Miralda-Escudé J., 2003, ApJ, 597, 66
Miralda-Escudé J., Rees M. J., 1994, MNRAS, 266, 343
Miralda-Escudé J., Cen R., Ostriker J. P., Rauch M., 1996, ApJ, 471, 582
Miralda-Escudé J., Haehnelt M., Rees M. J., 2000, ApJ, 530, 1
Olive K. A., Skillman E. D., 2004, ApJ, 617, 29
Paschos P., Norman M. L., Bordner J. O., Harkness R., 2007, preprint (arXiv:0711.1904)
Pawlik A. H., Schaye J., van Scherpenzeel E., 2009, MNRAS, in press (arXiv:0807.3963)
Petitjean P., Webb J. K., Rauch M., Carswell R. F., Lanzetta K., 1993, MNRAS, 262, 499
Rauch M. et al., 1997, ApJ, 489, 7
Ricotti M., Gnedin N. Y., Shull J. M., 2000, ApJ, 534, 41
Schaye J., 2001, ApJ, 559, 507
Schaye J., Theuns T., Rauch M., Efstathiou G., Sargent W. L. W., 2000, MNRAS, 318, 817
Schaye J., Aguirre A., Kim T., Theuns T., Rauch M., Sargent W. L. W., 2003, ApJ, 596, 768
Shull J. M., Tumlinson J., Giroux M. L., Kriss G. A., Reimers D., 2004, ApJ, 600, 570
Springel V., 2005, MNRAS, 364, 1105
Storrie-Lombardi L. J., McMahon R. G., Irwin M. J., Hazard C., 1994, ApJ, 427, L13
Syphers D. et al., 2009, ApJ, 690, 1181
Telfer R. C., Zheng W., Kriss G. A., Davidsen A. F., 2002, ApJ, 565, 773
Tepper García T., 2006, MNRAS, 369, 2025
Theuns T., 2005, in Williams P., Shu C.-G., Menard B., eds, IAU Colloq. 199, Probing Galaxies Through Quasar Absorption Lines. Cambridge Univ. Press, Cambridge, p. 185
Theuns T., Leonard A., Efstathiou G., Pearce F. R., Thomas P. A., 1998, MNRAS, 301, 478
Theuns T., Schaye J., Haehnelt M. G., 2000, MNRAS, 315, 600
Theuns T., Bernardi M., Frieman J., Hewett P., Schaye J., Sheth R. K., Subbarao M., 2002, ApJ, 574, L111 (T02)
Tittley E. R., Meiksin A., 2007, MNRAS, 380, 1369
Tytler D. et al., 2004, ApJ, 617, 1
Valageas P., Schaeffer R., Silk J., 2002, A&A, 388, 741
Weinberg D. H. et al., 1999, in Banday A. J., Sheth R. K., da Costa L. N., eds, Proc. MPA-ESO Cosmology Conf., Evolution of Large Scale Structure: From Recombination to Garching. Print Partners Ipskamp, Enschede, p. 346
Wiersma R. P. C., Schaye J., Smith B. D., 2009, MNRAS, 393, 99
Zhang Y., Anninos P., Norman M. L., 1995, ApJ, 453, L57
Zheng W., Chiu K., Anderson S. F., Schneider D. P., Hogan C. J., York D. G., Burles S., Brinkmann J., 2004, AJ, 127, 656

This paper has been typeset from a TEX/LATEX file prepared by the author.